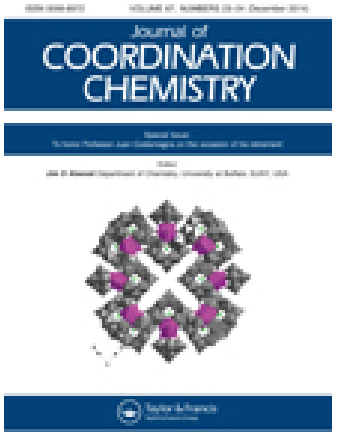

Journal of Coordination Chemistry
Publication details, including instructions for authors and subscription information:
http://www.tandfonline.com/loi/gcoo20

Copper(II) complexes of 2-amino-5-chloro-3-fluoropyridine: syntheses and magnetic properties of $(3,5\text{-FCAP})_2CuX_2$ and $(3,5\text{-FCAPH})_2CuX_4$

Benjamin L. Solomon[a], Christopher P. Landee[b], Mark M. Turnbull[a] & Jan L. Wikaira[c]

[a] Carlson School of Chemistry and Biochemistry, Clark University, Worcester, MA, USA

[b] Department of Physics, Clark University, Worcester, MA, USA

[c] Department of Chemistry, University of Canterbury, Christchurch, New Zealand

Accepted author version posted online: 14 Feb 2014.Published online: 12 Mar 2014.

To cite this article: Benjamin L. Solomon, Christopher P. Landee, Mark M. Turnbull & Jan L. Wikaira (2014) Copper(II) complexes of 2-amino-5-chloro-3-fluoropyridine: syntheses and magnetic properties of $(3,5\text{-FCAP})_2CuX_2$ and $(3,5\text{-FCAPH})_2CuX_4$, Journal of Coordination Chemistry, 67:23-24, 3953-3971, DOI: 10.1080/00958972.2014.893431

To link to this article: http://dx.doi.org/10.1080/00958972.2014.893431

Journal of Coordination Chemistry, 2014
Vol. 67, Nos. 23–24, 3953–3971, http://dx.doi.org/10.1080/00958972.2014.893431

Copper(II) complexes of 2-amino-5-chloro-3-fluoropyridine: syntheses and magnetic properties of $(3,5\text{-FCAP})_2CuX_2$ and $(3,5\text{-FCAPH})_2CuX_4$

BENJAMIN L. SOLOMON†, CHRISTOPHER P. LANDEE‡, MARK M. TURNBULL*† and JAN L. WIKAIRA§

†Carlson School of Chemistry and Biochemistry, Clark University, Worcester, MA, USA
‡Department of Physics, Clark University, Worcester, MA, USA
§Department of Chemistry, University of Canterbury, Christchurch, New Zealand

(*Received 20 September 2013; accepted 9 January 2014*)

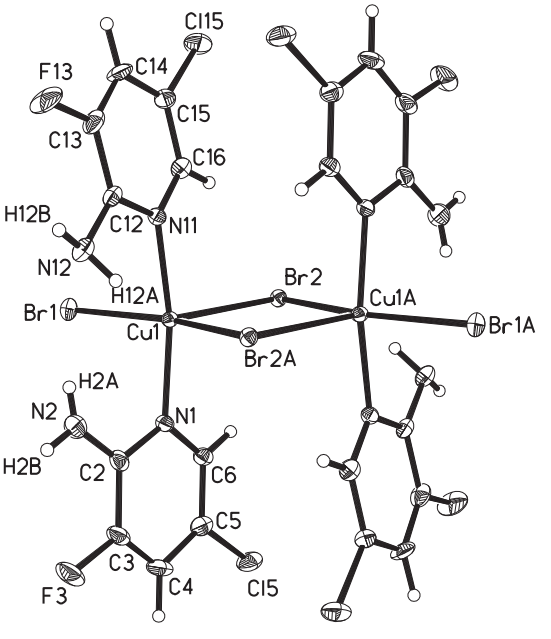

The reaction of 2-amino-5-chloro-3-fluoropyridine (3,5-FCAP) with copper(II) halides in neutral or acidic media gave the complexes $(3,5\text{-FCAP})_2CuX_2$ and $(3,5\text{-FCAPH})_2CuX_4$ (X = Cl, Br). Variable temperature magnetic susceptibility reveals anti-ferromagnetic interactions, *J*, ranging from −0.9 to −31.3 K.

Using 2-amino-5-chloro-3-fluoropyridine, two new copper halide coordination complexes and two new salts have been synthesized: $[(3,5\text{-FCAP})_2CuCl_2]$ (**1**), $[(3,5\text{-FCAP})_2CuBr_2]$(**2**), $(3,5\text{-FCAPH})_2[CuCl_4]$ (**3**) and $(3,5\text{-FCAPH})_2[CuBr_4]$ (**4**) [3,5-FCAP = 2-amino-5-chloro-3-fluoropyridine; 3,5-FCAPH = 2-amino-5-chloro-3-fluoropyridinium]. These complexes have been analyzed through

*Corresponding author. Email: mturnbull@clarku.edu

single-crystal X-ray diffraction and temperature-dependent magnetic susceptibility. Compounds **1** and **2** crystallize in the triclinic space group *P-1*, while **3** and **4** crystallize in the monoclinic space group $P2_1/c$. All structures were distinct, with **1** giving a bihalide bridged chain, **2** yielding a halide bridged dimer, **3** forming a two-halide bridged chain via short Cl···Cl contacts, and **4** producing a rectangular sheet via short Br···Br contacts. All four compounds exhibit anti-ferromagnetic interactions and were fit to linear chain (**1** and **3**), dimer (**2**), and rectangular 2-D sheet (**4**) models. The resulting J/k_B values are −3.4(1), −31.3(8), −0.9(1), and −9.46(6) K with an α value ($\alpha = J'/J$) of 0.06(2), respectively.

Keywords: Cu(II) salts and complexes; Magnetic interactions; Pyridine complexes; X-ray structures

1. Introduction

Synthesis and studies of the structures and corresponding magnetic exchange properties of copper(II) halide coordination complexes and salts have been of interest to our research group for quite some time [1–4]. These systems merit study due to the low-dimensional anti-ferromagnetic exchange observed and the opportunity to compare and contrast packing motifs to gain insight into magneto-structural correlations. One impetus to investigate low-dimensional anti-ferromagnets resides with the connection between the dimensionality of high-temperature superconductive materials, such as 2-D copper oxide layers, and the phase transition that makes them superconducting [5, 6].

In order to correlate relationships between magnetic interactions and physical structure, families of compounds with the formula $[A_2CuX_2]$ and $(AH)_2[CuX_4]$, where A is an organic compound that can behave as a base or neutral ligand and X is a halide (Cl or Br), are synthesized. Pyridine and pyridine derivatives have proven to be suitable compounds that can aid in the formation of packing structures by the addition of different substituents to the ring [7–9]. Substituent position on the ring is also important as it affects hydrogen bond formation and other intermolecular interactions [10]. Methyl [11–13], amino [14–16], and other [1, 17] groups have been used as substituents on pyridine rings in Cu(II) complexes that have been studied previously. These substituents modify the packing structure through the respective size of the substituent, through the introduction of possible hydrogen bond donors and acceptors into the complex, and through increased or decreased electron density in the pyridine ring.

Magnetic super exchange pathways can be mediated through intermediate diamagnetic atoms. Ligands can influence the superexchange pathway between Cu ions by providing pathways for moments to couple through intermolecular interactions.

Halides provide viable superexchange pathways between Cu(II) ions [18]. Examples include bihalide and two-halide bridges (scheme 1). However, when such a path is not present, substituents can aid in the formation of contacts that can form a superexchange pathway. For example, the protons on an amino substituent can hydrogen bond with two chlorides bonded to two separate Cu ions [19].

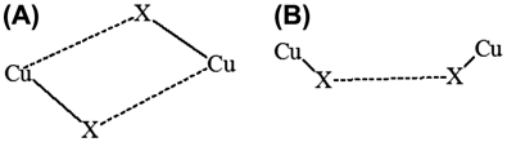

Scheme 1. Examples of a bihalide bridge (A) and a two-halide bridge (B). Dotted lines represent copper–halide contacts and halide–halide contacts.

A substituent that has not been utilized extensively for research into copper pyridine complexes and salts is fluorine. Fluorine is an excellent hydrogen bond acceptor and can change the packing structure and therefore magnetism of a Cu(II) complex. However, only three copper pyridine complexes using fluorine as a substituent have been synthesized and studied for magnetism and structural correlations: (2-amino-5-trifluoromethylpyridinium)$_2$[CuX_4] [20] (X = Cl or Br) and (2-amino-5-fluoropyridinium)$_2$[$CuCl_4$] [21]. This family must be expanded to determine the utility of fluorine as a substituent for directing crystal packing and, as a result, magnetic interactions. In order to extend this family of fluoropyridine Cu(II) compounds, salts and neutral complexes using 2-amino-5-chloro-3-fluoropyridine have been investigated. Here, we report the syntheses, structures, and magnetic properties of [(3,5-FCAP)$_2$$CuX_2$] and (3,5-FCAPH)$_2$[$CuX_4$] (3,5-FCAP = 2-amino-5-chloro-3-fluoropyridine).

2. Experimental setup

2-Amino-5-chloro-3-fluoropyridine was purchased from Matrix Scientific, copper bromide was purchased from Aldrich Chemical Company, and copper chloride, HCl, and HBr were obtained from Baker; all were used without purification. Elemental analyses were carried out by Marine Science Institute, University of California, Santa Barbara, CA 93106. IR spectra were recorded as KBr pellets on a Perkin-Elmer Spectrum 100.

2.1. *Synthesis*

2.1.1. Bis(2-amino-5-chloro-3-fluoropyridine)dichlorocopper(II) (1). $CuCl_2$ (0.0680 g, 0.506 mM) was dissolved in 13 mL of acetonitrile after 30 minutes of warming and stirring to yield a clear, yellowish-brown solution, which was allowed to cool. 2-Amino-5-chloro-3-fluoropyridine (0.1451 g, 0.990 mM) in 5 mL of acetonitrile was added to the $CuCl_2$ solution at room temperature. The clear, amber solution was left to evaporate at room temperature. Brown needle-like crystals were recovered by vacuum filtration after one day, washed with cold acetonitrile, and allowed to air dry to give 0.1115 g (26%). CHN Calcd (found) for $C_{10}H_8N_4F_2Cl_4Cu$: C, 28.09(28.52); H, 1.88(2.05); N, 13.10(13.39) %. IR (KBr) ν-3437 s, 3326 s, 3191 w, 1638 s (δ HNH), 1600 m, 1509 s, 1425 w, 1342 m, 1206 m, 1091 w, 940 w, 879 m, 805 w, 743 w, 687 w, 567 w, 499 w cm^{-1}.

2.1.2. Bis(2-amino-5-chloro-3-fluoropyridine)dibromocopper(II) (2). $CuBr_2$ (0.1198 g, 0.536 mM) in 11 mL of acetonitrile was added to 2-amino-5-chloro-3-fluoropyridine (0.1498 g, 1.02 mM) in 5 mL of acetonitrile, generating a dark green solution, which was left to evaporate at room temperature. After one week, dark prisms (purple when crushed) were recovered by vacuum filtration, washed with cold acetonitrile, and allowed to air dry to give 0.1891 g (35%). Single crystals (dark plates) were grown through recrystallization of the prisms from acetonitrile. CHN Calcd (found) for $C_{10}H_8N_4F_2Cl_2CuBr_2$: C, 23.26(23.08); H, 1.56(1.74); N, 10.84(10.36) %. IR (KBr) ν-3330 br, 1634 s (δ HNH), 1601 m, 1574 w, 1485 s, 1419 m, 1338 w, 1207 s, 1094 w, 936 m, 890 w, 880 m, 802 w, 697 w, 566 w cm^{-1}.

2.1.3. Bis(2-amino-5-chloro-3-fluoropyridinium) tetrachlorocuprate(II) (3). $CuCl_2$ (0.0660 g, 0.491 mM) in 2 mL of water was added to 2-amino-5-chloro-3-fluoropyridine

(0.1496 g, 1.02 mM) in 1.7 mL of 6 M HCl, yielding a clear, forest-green solution, which was left to evaporate at room temperature. After one month, a green single crystal (0.0319 g, 6.2%) was recovered from the solution and manually dried to remove any residual supernate. Upon prolonged exposure to oxygen, the surface of the crystal turned red, but the interior remained green. A larger green single crystal was produced from the supernate after an additional two weeks. The crystal weighed 0.0756 g (14.6%) for a total yield of 20.8%. CHN Calcd (found) for $C_{10}H_{10}N_4F_2Cl_6Cu$: C, 24.00(24.38); H, 2.01(2.16); N, 11.19(11.28) %. IR (KBr) ν-3337 m, 3289 m, 3220 m, 3151 m, 3076 m, 2992 m (ν N–H, C–H) 1673 s (δ HNH), 1613 s, 1567 m, 1186 m, 936 m, 662 m cm^{-1}.

2.1.4. Bis(2-amino-5-chloro-3-fluoropyridinium) tetrabromocuprate(II) (4). $CuBr_2$ (0.1295 g, 0.0579 mM) in 2 mL of water was added to 2-amino-5-chloro-3-fluoropyridine (0.1402 g, 0.0957 mM) in 2.6 mL of 6 M HBr, yielding a dark red solution which was left to evaporate at room temperature until the volume reduced to 2 mL (~three months) and was subsequently placed in a desiccator. After six weeks, purple plates were recovered by vacuum filtration, washed with cold water, and allowed to air dry to give 0.2298 g (33%). CHN Calcd (found) for $C_{10}H_{10}N_4F_2Cl_2CuBr_4$: C, 17.71(17.51); H, 1.48(1.82); N, 8.25(7.92) %. IR (KBr) ν-3289 m, 3238 m, 3147 m, 3037 m (ν N–H, C–H) 1669 s (δ HNH), 1615 s, 1567 s, 1411 m, 1339 m, 1281 m, 1190 m, 937 m, 802 w, 757 w, 663 w, 563 w cm^{-1}.

2.2. *X-ray data collection*

Data for **1–4** were collected on an Agilent Technologies/CrysAlisPro system with Cu Kα radiation ($\lambda = 1.5418$ Å) using ω scans for data collection at 120.0(1) K. Cell parameters were determined and refined using CrysAlisPro [22]. Absorption corrections were made via SADABS [23]. The structures were solved by direct methods and refined via least-squares analysis using SHELX97-2 [24]. All nonhydrogen atoms were refined anisotropically. Hydrogen atoms bonded to N were located in the difference maps and their positions refined using fixed isotropic thermal parameters. Hydrogen atoms bonded to C were located geometrically and refined using a riding model with fixed isotropic U-values. Crystallographic data may be found in table 1. Selected bond lengths and angles are given in table 2. Hydrogen bond data are given in table 3. The structures have been deposited in the CCDC (**1**, 952164; **2**, 952165; **3**, 952166; **4**, 952167). A Bruker D8 powder X-ray diffractometer was used to verify that powder samples used for magnetic measurements were pure and the same phase as the single crystal.

2.3. *Magnetic susceptibility data collection*

Magnetic data were collected using a Quantum Design MPMS-XL SQUID magnetometer. Finely ground samples of the crystals were packed into gelatin capsules. The magnetic moment was measured as a function of field from 0 to 50 kOe at 1.8 K. Several data points were also collected as the field was brought back to 0 kOe to check for hysteresis; none was observed. Temperature-dependent magnetization data were collected in a 1 kOe field from 1.8 to 310 K. The contribution from the sample holder was measured separately and subtracted from all data-sets. A temperature-independent magnetism correction of 60×10^{-6} for copper(II) was applied. Diamagnetic corrections were estimated from Pascal's constants [25].

Table 1. X-ray data for **1–4**. Large peaks and holes in **4** are less than 1 Å away from bromides.

Compound	**1**	**2**	**3**	**4**
Empirical formula	$C_{10}H_8N_4F_2Cl_4Cu$	$C_{10}H_8N_4F_2Cl_2CuBr_2$	$C_{10}H_{10}N_4F_2Cl_6Cu$	$C_{10}H_{10}N_4F_2Cl_2CuBr_4$
Molecular weight	427.54	516.46	500.46	678.3
Crystal system	Triclinic	Triclinic	Monoclinic	Monoclinic
Space group	*P-1*	*P-1*	$P2_1/c$	$P2_1/c$
a (Å)	3.8337(3)	6.7932(5)	8.1857(3)	8.42756(18)
b (Å)	7.5886(8)	10.1538(9)	8.0077(3)	13.5129(3)
c (Å)	12.6478(13)	12.2696(8)	13.1978(4)	16.9097(4)
α (°)	104.996(9)	106.774(7)	90	90
β (°)	92.710(7)	93.631(6)	97.348(3)	101.988(2)
γ (°)	92.586(8)	107.946(7)	90	90
T (K)	120.01(10)	120.01(10)	120.01(10)	120.00(10)
λ (Å)	1.54184	1.54184	1.54184	1.54184
V (Å^3)	354.40(6)	760.04(10)	858.00(5)	1883.69(7)
Z	1	2	2	4
D_{Calcd} (Mg/m^3)	2.003	2.257	1.937	2.392
Absorption coefficient (mm^{-1})	9.318	11.616	10.607	14.385
F (0 0 0)	211	494	494	1276
Crystal size (mm)	0.56 × 0.05 × 0.03	0.18 × 0.18 × 0.18	0.4 × 0.3 × 0.1	0.2 × 0.12 × 0.04
θ_{min}, θ_{max} (°)	11.63, 74.12	3.82, 73.84	5.45, 73.72	4.22, 73.87
Index ranges	$-4 \le h \le 4$ $-9 \le k \le 9$ $-15 \le l \le 15$	$-8 \le h \le 8$ $-11 \le k \le 12$ $-15 \le l \le 11$	$-8 \le h \le 10$ $-9 \le k \le 7$ $-15 \le l \le 16$	$-8 \le h \le 10$ $-16 \le k \le 15$ $-20 \le l \le 20$
Reflections collected	2815	4115	2225	4756
Independent reflections	1172	2957	1627	3716
Max./min. trans. factors	1.00000/0.42857	1.00000/0.64980	1.00000/0.29042	1.00000/0.13927
No. of restraints/ parameters	0/103	2/206	1/113	0/226
Final *R1*, *wR2* [$I > 2\sigma(I)$]	0.0318, 0.0824	0.0224, 0.0625	0.0351, 0.0977	0.0468, 0.1406
Goodness-of-fit on F^2	1.058	1.098	1.076	1.14
Largest peak and hole (e Å^{-3})	0.46 and −0.38	0.42 and −0.69	0.56 and −1.04	1.24 and −1.46

3. Results and discussion

Reaction of CuX_2 with 3,5-FCAP in acetonitrile yielded [(3,5-FCAP)$_2$CuX$_2$] (scheme 2) [X = Cl (**1**), Br (**2**)] in yields of 26 and 35%, respectively. Crystals of **1** suitable for X-ray diffraction were obtained by slow evaporation of the solutions. Suitable crystals of **2** were obtained from recrystallization of the original product in acetonitrile.

Similarly, reaction of CuX_2 with 3,5-FCAP in aqueous HX yielded [(3,5-FCAPH)CuX_4] (scheme 3) [X = Cl (**3**), Br (**4**)] in yields of 21% and 33%, respectively. Crystals of **3** and **4** suitable for X-ray diffraction were obtained by slow evaporation of the aqueous solutions.

3.1. *Crystal structure analysis*

3.1.1. [(3,5-FCAP)$_2$CuCl$_2$] (1). Compound **1** crystallizes in the triclinic space group *P-1*. The molecular unit is shown in figure 1. The copper ion lies on a crystallographic inversion center and has a nearly square planar geometry with a 91.06(6)° N1–Cu–Cl1 bond angle with trans angles of 180° as required by the symmetry. The Cu–Cl1 bond length is 2.2594 (7) Å, typical of other substituted dichlorocopper pyridine compounds, which have bond

Table 2. Bond lengths (Å) and angles (°) for **1–4**.

Bond lengths	**1**	**2**	**3**	**4**
Cu–X1	2.2594(7)	2.4220(5)	2.2621(5)	2.3782(9)
Cu–X2		2.6754(5)	2.2775(6)	2.3920(9)
Cu–X2A		2.5265(5)		
Cu–X3				2.3721(9)
Cu–X4				2.3844(9)
Cu–N1/Cu–N11	2.085(2)	2.014(2)/2.017(2)		
N1–C2/N11–C12	1.348(4)	1.356(4)/1.350(3)	1.345(3)	1.349(7)/1.335(7)
N1–C6/N11–C16	1.361(3)	1.350(4)/1.350(4)	1.365(3)	1.366(8)/1.373(7)
C2–N2/C12–N12	1.335(4)	1.344(4)/1.367(4)	1.326(3)	1.332(7)/1.330(7)
C3–F3/C13–F13	1.350(3)	1.349(3)/1.353(3)	1.336(3)	1.345(6)/1.339(7)
C5–Cl5/C15–Cl15	1.731(3)	1.735(3)/1.731(3)	1.728(2)	1.720(6)/1.725(5)
N1–H1/N11–H11			0.79(3)	0.92(8)/0.88(8)
Bond angles	**1**	**2**	**3**	**4**
X1–Cu–X2		158.45(2)	89.41(2)	96.03(3)
X1–Cu–X1A	180			
X1–Cu–X2A		110.789(18)	90.59(2)	
X2–Cu–X2A		90.725(16)		
X1–Cu–X3				136.99(4)
X1–Cu–X4				97.25(3)
X2–Cu–X3				96.73(3)
X3–Cu–X4				98.42(3)
X1–Cu–N1/X1–Cu–N11	91.06(6)	89.71(6)/86.97(6)		
N1–Cu–N11		167.02(10)		
C2–N1–C6/C12–N11–C16	118.2(2)	119.6(2)/119.7(2)	124.3(2)	124.3(5)/123.9(5)

Table 3. Hydrogen bonding parameters for **1–4**.

D–H···A	*d*(D–H)	*d*(H···A)	*d*(D···A)	∠(DHA)
Compound ***1***				
N2–H2A···Cl1A	0.82(4)	2.40(4)	3.197(3)	162(4)
N2–H2B···Cl1B	0.87(4)	2.56(4)	3.295(3)	143(4)
Compound **2**				
N2–H2B···Br1C	0.83(2)	2.75(2)	3.495(3)	150(3)
N12–H12B···Br1A	0.84(4)	2.70(4)	3.500(3)	159(3)
N12–H12A···Br2D	0.82(4)	2.66(4)	3.388(3)	148(3)
N12–H12B···F13	0.84(4)	2.32(3)	2.741(3)	111(3)
Compound **3**				
N1–H1···Cl1	0.79(3)	2.61(3)	3.217(2)	134(3)
N1–H1···Cl2	0.79(3)	2.60(3)	3.310(2)	150(3)
N2–H2A···Cl2	0.82(2)	2.51(2)	3.255(2)	151(3)
N2–H2B···Cl1E	0.90(4)	2.34(4)	3.222(2)	166(3)
Compound **4**				
N1–H1···Br1	0.92(8)	2.63(7)	3.337(5)	134(6)
N1–H1···Br2	0.92(8)	2.88(7)	3.664(5)	145(6)
N2–H2A···Br2	0.84(8)	2.59(8)	3.400(5)	163(7)
N2–H2B···Br1A	0.84(8)	2.61(8)	3.449(6)	175(7)
N11–H11···Br3A	0.88(8)	2.66(7)	3.330(5)	134(6)
N12–H12B···Br3	0.85(8)	2.68(8)	3.497(6)	164(7)
N12–H12A···Br4A	0.82(8)	2.61(9)	3.419(5)	172(7)

Note: Symmetry operations: A = $x+1$, y, z; B = $x+1$, y, $z+1$; C = $x+2$, $y+2$, $z+1$; D = $x+1$, $y+1$, $z+1$; E = x, $y-1$, z.

lengths ranging from 2.220 to 2.304 Å [26–28]. The substituted pyridine ring is nearly planar with a mean deviation of the constituent atoms of 0.0177 Å from the mean plane. N2 is 0.0965 Å out of the plane, which is most likely due to hydrogen bonding. Bond lengths and

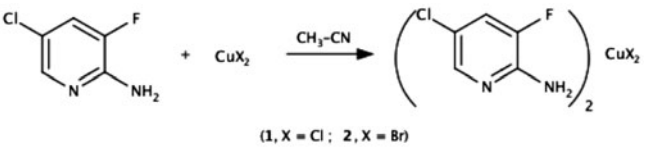

Scheme 2. Preparation of **1** and **2**.

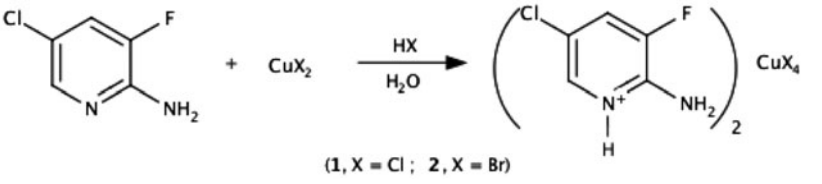

Scheme 3. Preparation of **3** and **4**.

angles within the pyridine ring are similar to those found in [(2-amino-3,5-dichloropyridine) $CuCl_2$] [29].

The only marked difference is the 3-position, where the C–F bond is ~0.2 Å shorter than the C–Cl bond as expected. The pyridine ring is canted 36.4° with respect to the normal of the copper coordination plane and inclined 13.0° from the Cu–N1 axis.

Compound **1** crystallizes as halide bi-bridged chains parallel to the *a*-axis (see figure 2). The chains are formed, parallel to the *a*-axis, by long Cu···Cl contacts (2.9745(6) Å). The Cu–Cl–Cu bridging angle is 93.18(2)°. Intermolecular hydrogen bonds through H2A with an N2···Cl1 distance of 3.197(3) Å help to stabilize the bi-bridged chains. H2B links the

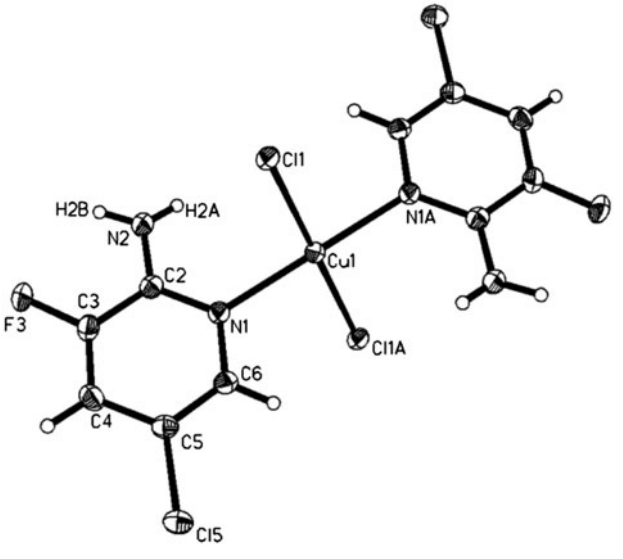

Figure 1. Thermal ellipsoid plot of the molecular unit of **1** showing 50% probability ellipsoids. Only the asymmetric unit, copper coordination sphere, and hydrogen atoms whose positions were refined are labeled.

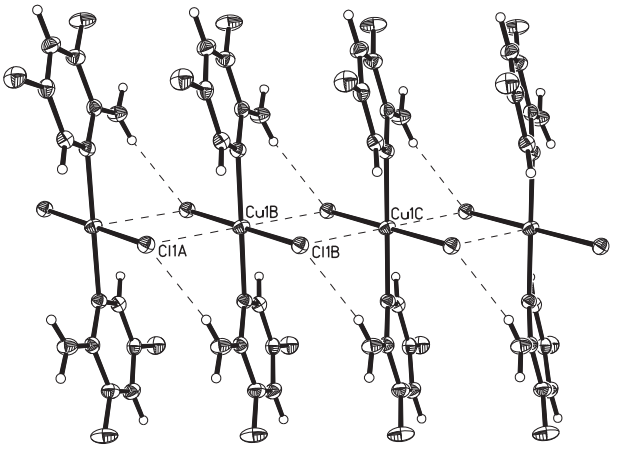

Figure 2. Chain structure of **1** formed by intermolecular Cu–Cl contacts, viewed parallel to the *c*-axis.

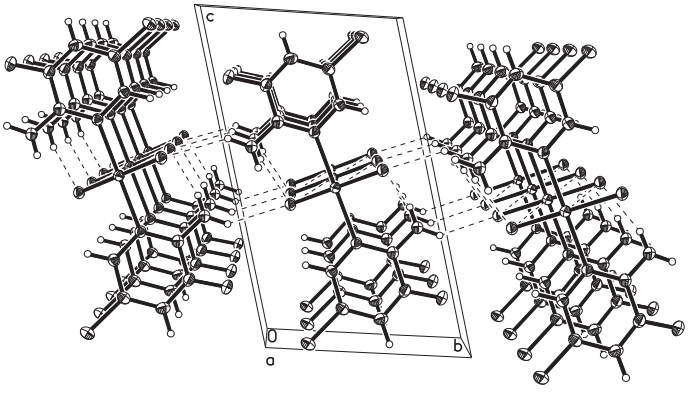

Figure 3. Packing diagram of **1** viewed parallel to the *a*-axis. Dotted lines represent hydrogen bonds and Cu···Cl contacts.

chains parallel to the *b*-axis through a second hydrogen bond and a N(2)···Cl(1) distance of 3.295(3) Å. The substituted pyridine rings adopt an *anti*-conformation with respect to the amino substituents to achieve these connectivities. Full hydrogen bond parameters are listed in table 3. The packing diagram of **1** shows hydrogen bonds linking the chains (see figure 3).

3.1.2. [(3,5-FCAP)$_2$CuBr$_2$] (2). Compound **2** crystallizes in the triclinic space group *P-1*. There are two molecules in the unit cell which are situated across a crystallographic inversion center to form dimers (figure 4). The coordination geometry about each Cu(II) ion is square pyramidal based on the continuous symmetry measure with values of $S_{C4v} = 1.6$ (square pyramidal) compared to $S_{D3h} = 4.9$ (trigonal bipyramidal) [30, 31]. The Cu(II) ion sits 0.212 Å above the mean coordination plane. The *trans* N and Br angles about the copper ion are 167.02(10)° for N1–Cu–N11 and 158.45(2)° for Br1–Cu–Br2. The bromide bridges provide an axial/equatorial link between Cu ions and the Cu–Br bond lengths are

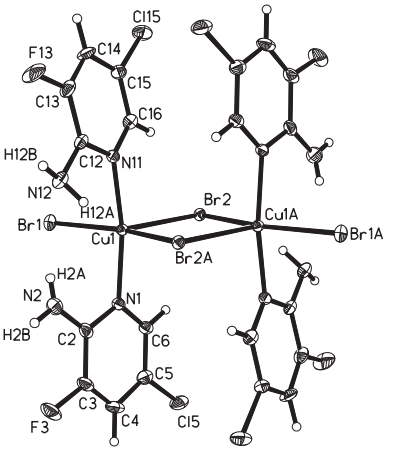

Figure 4. Thermal ellipsoid plot of the dimeric structure of **2** showing 50% probability ellipsoids. Only the asymmetric unit, copper coordination sphere, and hydrogen atoms whose positions were refined are labeled.

2.5265(5) for Cu–Br2A and 2.6754(5) for Cu–Br2, the axial and equatorial positions. The Cu–Br1 bond length is 2.4220(5) Å and falls within the 2.393–2.451 Å bond length range found in other substituted dibromocopper pyridine compounds [4, 32, 33]. The Cu–Br–Cu bridging angle is 89.275(16)°.

The N1 and N11 rings are nearly perpendicular to the dimer with bond angles of 88.15 (6)° for N1–Cu–Br2 and 90.34(6)° for N11–Cu–Br2. Short Br···Br contacts ($d_{\mathrm{Br\ldots Br}}$ = 3.742 Å, $\theta_{\mathrm{Cu–Br2\ldots Br2a}}$ = 120.9°) link dimers. A staggered chain of dimers is formed parallel to the *a*-axis through these contacts. Hydrogen bonding links one chain of dimers with the nearest chain through the H2B···Br1 contact and provides additional linkages for the same chains through the H12B···Br1 contact (see figure 5). An intramolecular fluorine hydrogen

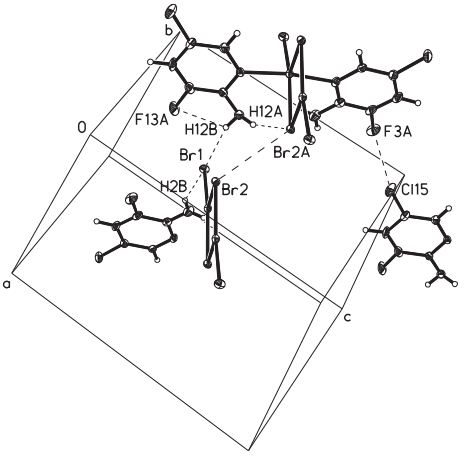

Figure 5. Thermal ellipsoid plot showing non-bonding contacts in **2**. Dotted lines represent hydrogen bonds and halogen–halogen contacts.

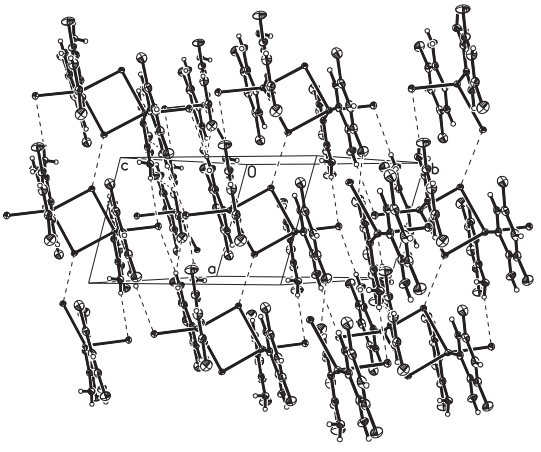

Figure 6. The crystal structure of **2** showing the formation of chains of dimers parallel to the *a*-axis via Br···Br contacts. Dotted lines represent hydrogen bonds and bromide–bromide contacts.

contact is also present in the structure (see table 3), but is likely the result of the proximity of the two substituents on the pyridine ring. Strong halogen bonds between Cl15···F3 ($d_{Cl5\ldots F3} = 2.999$ Å, $\theta_{C15–Cl15\ldots F3} = 163.3°$, and $\theta_{Cl15\ldots F3–C3} = 152.0°$) link chains of ligands parallel to the *c*-axis. These contacts are shown in figure 5. The full crystal structure is given in figure 6.

3.1.3. (3,5-FCAPH)$_2$[CuCl$_4$] (3). Compound **3** crystallizes in the monoclinic space group $P2_1/c$. The molecular unit is shown in figure 7. The copper ion again lies on a crystallographic inversion center, as for **1**. The bond lengths for Cu–Cl1 (2.2621(5) Å) and Cu1–Cl2 (2.2775(6) Å) are comparable to other tetrachlorocuprate salts [4, 34, 35]. The geometry about the copper ion is nearly square planar with a 89.42(2)° Cl1–Cu–Cl2 bond angle with

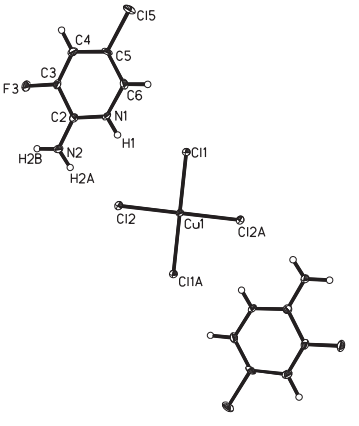

Figure 7. Thermal ellipsoid plot of the molecular unit of **3** showing 50% probability ellipsoids. Only the asymmetric unit, copper coordination sphere, and hydrogen atoms whose positions were refined are labeled.

Table 4. Contact parameters for halide–halide contacts in **3** and **4**. τ is the dihedral angle Cu–X1···X2–Cu.

Compound	X1	X2	X–X (Å)	Cu–X1···X2 (°)	X1···X2–Cu (°)	τ (°)
3	Cl2	Cl2	3.965	139.9	139.9	−180.0
4	Br1	Br3	4.385	111.9	105.0	154.0
	Br1	Br4	4.405	141.8	104.2	84.2
	Br2	Br4	4.142	149.5	147.1	−100.1

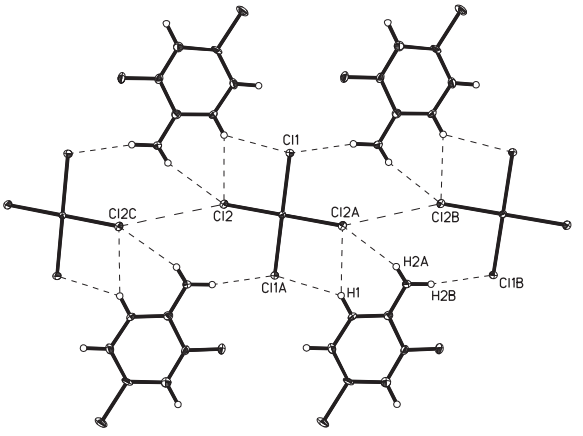

Figure 8. Geometry of 3,5-FCAPH cations about $[CuCl_4]^{2-}$ of **3**. Dotted lines represent hydrogen bonds and short chloride–chloride contacts.

trans angles of 180° as required by the symmetry. The pyridine rings are nearly planar with a deviation from the mean plane of 0.0051 Å. Bond lengths and angles within the ring are very similar to those found in the 2-amino-3,5-dichloropyridinium cation [36]. The only marked difference is in the 3-position, where the C–F bond is ~0.2 Å shorter than the C–Cl bond as expected.

Individual tetrachlorocuprate anions, related by unit cell translations, show close contacts (see table 4), forming two-halide bridged chains parallel to the *b*-axis (figure 8). Hydrogen bonds between the chloride ions of $[CuCl_4]^{2-}$ groups and both the amino and pyridinium hydrogens atoms of the 3,5-FCAPH ions stabilize the structure in the plane of the tetrachlorocuprate anions. Additionally, pyridinium ions that are hydrogen bonded to $[CuCl_4]^{2-}$ stabilize the packing structure via interactions between a halogen on the organic ion and a halide ion bonded to a copper ion as described by Willett [37, 38] and observed in related compounds (figure 8) [29, 34]. Contacts are observed between F3 and Cl2 ($d_{Cl2\ldots F3} = 3.224$ Å, $\theta_{Cu1-Cl2\ldots F3} = 99.5°$, and $\theta_{Cl2\ldots F3-C3} = 84.5°$) and symmetry related Cl5 ($d_{Cl\ldots Cl} = 3.304$ Å, $\theta_{C5-Cl5\ldots Cl5A} = 147.0°$). The chains are fairly well isolated as a distance of greater than 5.8 Å separates Cl1 from the closest chloride ion of the nearest chain. The crystal packs in sheets of cations and anions in an AABAAB fashion parallel to the *bc*-face (figure 9).

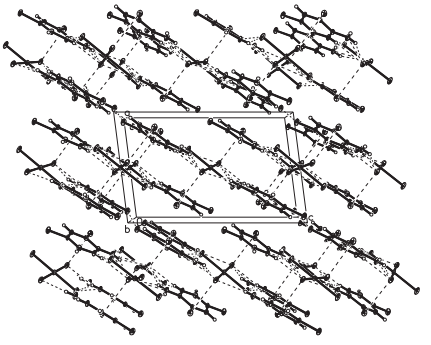

Figure 9. Crystal structure of **3** viewed parallel to the *b*-axis. Dotted lines represent hydrogen bonds and chloride–fluorine contacts.

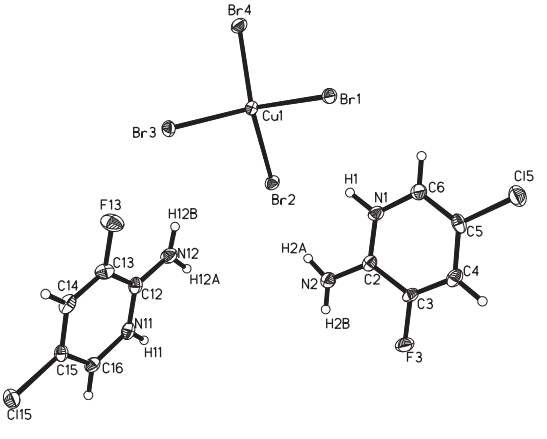

Figure 10. Thermal ellipsoid plot of the molecular unit of **4** showing 50% probability ellipsoids. Only hydrogen atoms whose positions were refined are labeled.

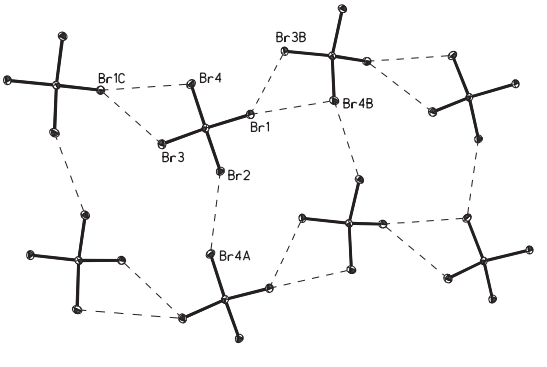

Figure 11. Rectangular structure of $CuBr_4^{2-}$ of **4** viewed perpendicular to the *ab*-face. Dotted lines represent bromide–bromide contacts.

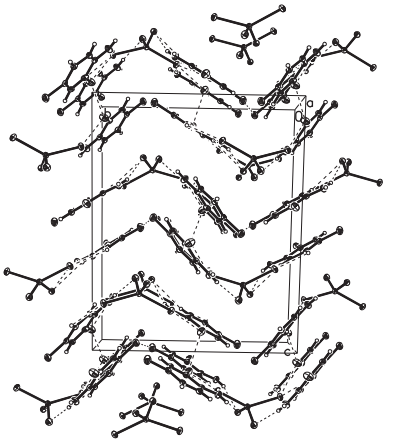

Figure 12. Crystal structure of **4** showing the pleated sheets formed by both $[CuBr_4]^{2-}$ and FCAPH in the crystal. Dotted lines represent hydrogen bonds and halogen···halogen contacts.

3.1.4. (3,5-FCAPH)$_2$[CuBr$_4$] (4). Compound **4** crystallizes in the monoclinic space group $P2_1/c$. The molecular unit is shown in figure 10. The Cu–Br bond lengths are nearly identical, ranging from 2.3721(9) to 2.3920(9) Å (see table 2). The tetrabromocuprate ion is significantly distorted from tetrahedral with a mean *trans* angle of 138.8(4)°. Bond lengths and angles within the 3,5-FCAPH ion are the same within experimental error to those seen in **3**. Both pyridinium rings are nearly planar (mean deviations of 0.0061 and 0.0097 Å for N1 and N11 rings, respectively). Compound **4** exhibits three short contacts between halides ions of tetrabromocuprate ions (see table 4, figure 11). These contacts form a pleated sheet of $CuBr_4^{2-}$ groups parallel to the *ab*-face. The structure is stabilized by multiple hydrogen bonds from 3,5-FCAPH ions (see table 3). The cations crystallize between the sheets of tetrabromocuprate ions and pack in an ABBA fashion (figure 12). Additionally, there are three halogen–halogen contacts and one halogen–halide contact present in the structure. There are halogen–halogen contacts between symmetry-related F3 atoms ($d_{F\ldots F} = 2.768$ Å and $\theta_{C3-F3\ldots F3a} = 102.6°$) and Cl5 and Cl15 ($d_{Cl\ldots Cl} = 3.576$ Å, $\theta_{C5-Cl5\ldots Cl15} = 138.8°$, and $\theta_{Cl5\ldots Cl15-C15} = 121.9°$). The contacts formed by F13 are bifurcated. F13 has contacts with itself via a unit cell translation ($d_{F\ldots F} = 2.715$ Å and $\theta_{C13-F13\ldots F13A} = 126.8°$) and Br3 ($d_{F\ldots Br} = 3.273$ Å, $\theta_{C13-F13\ldots Br3} = 131.4°$, and $\theta_{F13\ldots Br3-Cu} = 133.0°$).

3.2. *Magnetic studies*

Susceptibility data were collected for **1–4** from 1.8 to 310 K in a 1 kOe field. The data for **1** and **3** were fit to models for the $S = 1/2$ uniform anti-ferromagnetic chain using the Hamiltonian $\hat{H} = -\Sigma_{A,B} J_{AB} \hat{S}_A \cdot \hat{S}_B$ [39]. Included in the model were variables for a Weiss correction to account for interchain interactions and a possible paramagnetic impurity. The Weiss correction improved the quality of the fit slightly for **1**, but the value of θ indicates that interchain interactions are negligible. The even smaller θ value for **3** shows how well isolated the chains are. Data for **2** were fit to the model for an anti-ferromagnetic dimer [40] with a Weiss correction and paramagnetic impurity. The small value for θ indicates that interdimer interactions are negligible. The increase in magnetic susceptibility at very low temperatures is caused by a trace paramagnetic impurity. Data for **4** were fit to the rectangular 2-D-Heisenberg anti-ferromagnetic model [3]. The low value of α indicates that weak interactions

between the chains are present. Data for **4** were also fit to a uniform anti-ferromagnetic chain with a Weiss correction for interchain interactions, which gave a value for θ similar to $\alpha J/k_B$, but produced a poorer fit in the region of χ_{max}. Plots of χ_m *versus* T for **1–4** are shown in figures 13–16 along with the best fits to their respective models, with the best-fit parameters given in table 5. The data for **1–4** show good agreement with their respective models.

The magnetic susceptibilities of **1**, **3,** and **4** increase with decreasing temperature. A maximum at 2.3 K is observed in **1**, indicating weak anti-ferromagnetic interactions. Weak anti-ferromagnetic interactions are also present in **4**, where a maximum at 5.8 K is observed. Compound **3** exhibits very weak anti-ferromagnetic interactions with no maximum observed

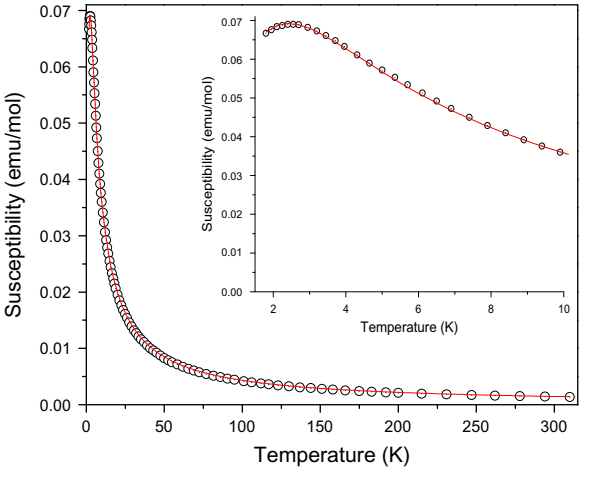

Figure 13. χ_m *vs.* T (○) data for **1** in a 1 kOe applied field. The solid line represents the best fit to a linear chain model. The inset shows an expansion from 1.5 to 10 K.

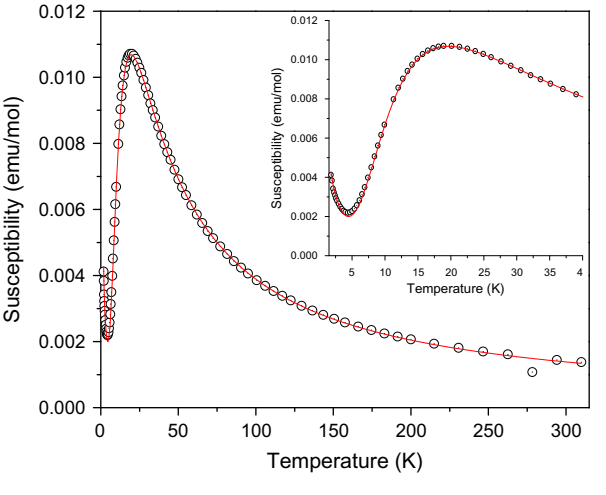

Figure 14. χ_m *vs.* T (○) data for **2** in a 1 kOe applied field. The solid line represents the best fit to a dimer model. The inset shows an expansion from 1.5 to 40 K.

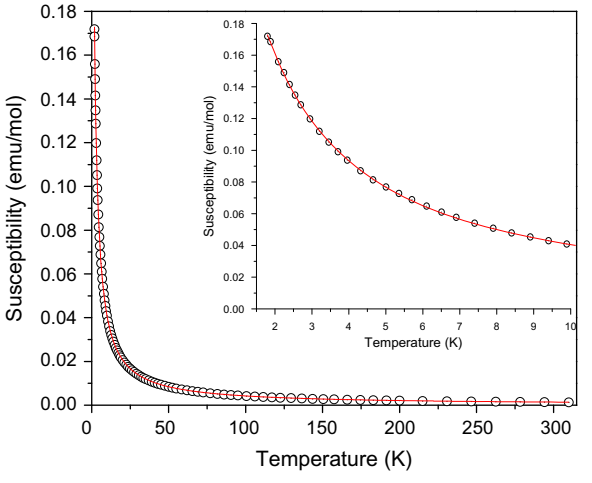

Figure 15. χ_m *vs.* T (○) data for **3** in a 1 kOe applied field. The solid line represents the best fit to a linear chain model. The inset shows an expansion from 1.5 to 10 K.

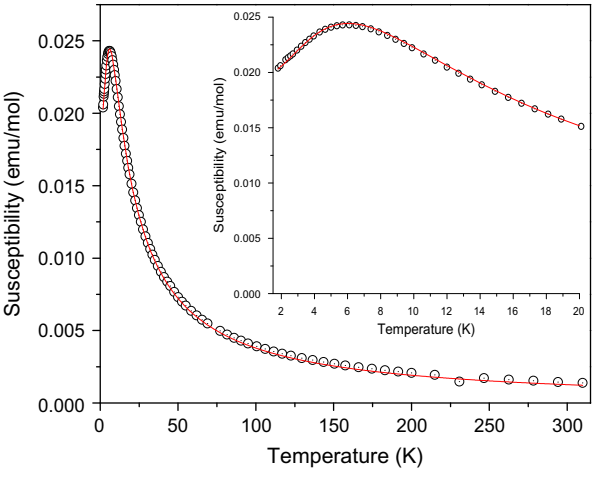

Figure 16. χ_m *vs.* T (○) data for **4** in a 1 kOe applied field. The solid line represents the best fit to a 2-D-Heisenberg rectangular model. The inset shows an expansion from 1.5 to 20 K.

at low temperatures. This results in an apparently high 'impurity' from the fitting of the magnetic data (as the magnetic exchange approaches zero, the data can be fit equally well to any magnetic model, or to an increasing % paramagnetic impurity, regardless of the chemical purity of the sample). No impurity was detected by powder X-ray diffraction. Compound **2** exhibits much stronger interactions than **1**, **3,** or **4**. The magnetic susceptibility of **2** increases with decreasing temperature until a maximum at 18.6 K is observed. The susceptibility then decreases very sharply, indicating a singlet ground state as expected for a dimer.

Table 5. Best-fit parameters to the respective models for **1**–**4**. *P* represents the % paramagnetic impurity in the sample, θ is the Weiss constant, and α is the ratio of the weak exchange constant to the strong exchange constant in the rectangular model ($0 < \alpha < 1$).

Compound	Model	C	J/k_B (K)	θ	α (J'/J)	p (%)	R^2
1	Chain	0.4417(9)	−3.4(1)	−0.27(9)		0.041(6)	0.9998
2	Dimer	0.428(6)	−31.3(8)	−1.0(9)		1.82(4)	0.994
3	Chain	0.427(1)	−1.07(1)	−0.01(7)		5.69(4)	0.9996
	C–W	0.428(2)		−0.6(3)		0.6(2)	0.9999
4	Rect.	0.402(1)	−9.46(6)	−0.220(1)	0.062(2)	0.999(1)	0.9996
	Chain	0.398(1)	−9.60(5)			0.498(1)	0.9997

3.3. *Discussion*

Neutral **1** and **2** crystallize in the triclinic space group *P-1*, while **3** and **4** crystallize in the monoclinic space group $P2_1/c$. Each compound is unique in terms of its packing structure, with **1** producing a bi-bridged chain network, **2** yielding a dimer, **3** producing a two-halide bridged chain, and **4** giving a rectangular sheet via halide···halide contacts.

Compound **1** is isostructural with the halide bi-bridged chains formed by [(2-amino-3,5-dichloropyridine)$_2$CuX$_2$] (X = Cl, Br) [29]. By replacing chlorine in the 3-position with fluorine, there has not been a significant structural change. However, in the case of the copper bromide complex, **2**, a dimeric structure is formed. A major factor influencing the structure of **2** is that the pyridine ligands adopt a *syn* conformation with respect to the amino substituents instead of the *anti*-conformation present in **1**. In the *syn* conformation, the amino substituents effectively block one face of the Cu(II) ion, preventing adjacent molecules from approaching each other on that side, thus limiting the bi-halide bridging to formation of a dimeric structure rather than a chain. This has been observed previously in related structures [4, 11, 41]. In **1**, the fluorine substituents do not participate in halogen or hydrogen bonding, so the halogen and hydrogen bonds made by the fluorine substituents in **2** may influence the change from *anti* to *syn*. In **2**, an intramolecular hydrogen bond is formed between fluorine and a proton on the amino substituent on the N11 ring, and a halogen bond is present between the fluorine on the N1 ring and the chlorine on the N11 ring. These contacts influence the packing pattern of **2** to give a *syn* conformation for the ligands and a dimer for the complex. Although magnetic interactions in halide bi-bridged dimers have not been studied in the same detail as their hydroxide bridged cousins [42], several such compounds have been reported, including two chloride bi-bridged dimers with exchange constants of −17 and −23 K [43] in good agreement with the exchange in **2**. The variety of structure and magnetic exchange exhibited in copper(II) bromide systems can be seen by comparison to a recently published monobromide-bridged complex where even though the overall coordination geometry at the Cu(II) centers is similar, the geometry of the bromide-supported bridges is sufficiently modified to support significant ferromagnetic exchange [44].

Another aspect to consider, in the structural difference between **1** and **2**, is that bromide is a poorer hydrogen bond acceptor and forms stronger halogen bonds than chloride [45, 46]. Compound **1** exhibits hydrogen bonds between the chloride ions and both protons on the amino substituent to stabilize the bi-bridged chain structure. Only Br1 in **2** is involved in a hydrogen bond, while Br2 (the bromide that forms the dimer) forms a halogen bond with a symmetry-related Br2.

Compound **3** is isostructural with the two-halide chains formed by (2-amino-3,5-dichloropyridinium)$_2$[CuX_4] (X = Cl, Br) [34]. By replacing the chlorine in the 3-position with fluorine, there has not been a significant structural change in the tetrachlorocuprate complex. The magnetic interactions are particularly weak in **3**. The crystal packing suggests a linear chain magnetic structure arising from Cl···Cl through space interactions and the data were fit to that model yielding the anticipated weak exchange and a negligible value for the interchain exchange (approximated using a Curie–Weiss correction). A fit of the $1/\chi$ (T) data to the Curie–Weiss law itself yielded comparable results (table 5), confirming the vanishingly weak exchange. However, in the case of **4**, a rectangular sheet is formed for the tetrabromocuprate complex, rather than a chain structure. The weaker hydrogen bonds and stronger halogen bonds formed by the bromide ions influence this change in packing. There is only one chloride–chloride contact present in **3** because hydrogen bond formation to chloride ions by amino and pyridinium protons effectively blocks the formation of short Cl1···Cl1 contacts, creating isolated tetrachlorocuprate chains. In **4**, hydrogen bonds are more numerous, but weaker than in **3**, and three bromide–bromide contacts are formed to yield a rectangular sheet. Weaker hydrogen bonds also allow 3,5-FCAPH ions to attain geometries not present in **3**. In **4**, fluorine atoms account for a single halogen–halide contact and two halogen–halogen contacts, with an additional contact between chlorines. Compound **3** contains two halogen–halogen contacts, which are stronger than the halogen–halogen contacts present in **4**. However, the two additional halogen–halide contacts in **4** modify the crystal packing and aid in the formation of the pleated sheets. The magnetic data were fit to both the rectangular model and a uniform chain model using a Curie–Weiss correction to account for interchain interactions and, as expected, are larger for the bromide complex, **4**, than for **3**. The fitted exchange values from the two models are nearly the same within experimental error. This correlates well with the structural aspects. The strength of the magnetic exchange via the two-halide pathway is affected not only by the halide…halide distance but also by the Cu–X…X angles, with larger exchange seen as the angle approaches 180° [18]. Analysis of the contacts in **4** shows that although there are three potential contacts based solely on Br…Br distances, one is anticipated to be significantly stronger as it has the shortest Br…Br distance and the largest Cu–Br…Br angles. This is in agreement with the fitted data showing only one significant magnetic exchange pathway.

These new compounds expand the variety of lattice types in copper halide pyridine complexes that use fluorine as a substituent. Prior to the preparation and characterization of **1–4**, only distorted honeycomb lattices and ladder motifs had been observed [20, 21]. 2-Amino-3,5-dichloropyridine and 2-amino-3,5-dibromopyridine produced isostructural coordination complexes when changing the halide from Cl to Br [29]. This was also the case for the tetrachlorocuprates and tetrabromocuprates produced by the protonated form of these organic species [34]. This was not the case for 3,5-FCAP, as changing the halide produced changes in both the structures and magnetic properties of the materials. Although copper chloride and bromide compounds are frequently isostructural, the differences observed here are not unique [4, 20, 41]. What is unique is the specific effects of fluorine in terms of nonbonding contacts and its effect on crystal structures. By comparing fluorine to other substituents, greater insight is gained into crystal packing patterns and consequent magnetic interactions. This suggests that further work is needed to study how replacing substituents with fluorine can tune the crystal structure and magnetic properties.

Acknowledgements

The Bruker D8-Advance powder X-ray diffractometer was purchased with the assistance of Funds from the Kresge Foundation and PCISynthesis, Inc. BLS is grateful for support from a PCISynthesis, Inc. Summer Research Fellowship.

Funding

The MPMS-XL SQUID magnetometer was purchased with the assistance of funds from the National Science Foundation (IMR-0314773) and the Kresge Foundation.

References

[1] W. Zhang, J.R. Jeitler, M.M. Turnbull, C.P. Landee, M. Wei, R.D. Willett. *Inorg. Chim. Acta*, **256**, 183 (1997).
[2] C. Landee, M. Turnbull, C. Galeriu, J. Giantsidis, F. Woodward. *Phys. Rev. B*, **63**, 100402 (2001).
[3] R.T. Butcher, C.P. Landee, M.M. Turnbull, F. Xiao. *Inorg. Chim. Acta*, **361**, 3654 (2008).
[4] M. Abdalrahman, C.P. Landee, S.G. Telfer, M.M. Turnbull, J.L. Wikaira. *Inorg. Chim. Acta*, **389**, 66 (2012).
[5] J.G. Bednorz, K.A. Müller. *Z. Phys. B*, **64**, 189 (1986).
[6] M. Wu, J. Ashburn, C. Torng, P. Hor, R. Meng, L. Gao, Z. Huang, Y. Wang, C. Chu. *Phys. Rev. Lett.*, **58**, 908 (1987).
[7] B.O. Patrick, C.L. Stevens, A. Storr, R.C. Thompson. *Polyhedron*, **22**, 3025 (2003).
[8] G.A. van Albada, I. Mutikainen, U. Turpeinen, J. Reedijk. *Polyhedron*, **23**, 993 (2004).
[9] B. Żurowska, J. Mroziński, K. Ślepokura. *Polyhedron*, **26**, 3379 (2007).
[10] E. Peris, J.C. Lee, J.R. Rambo, O. Eisenstein, R.H. Crabtree. *J. Am. Chem. Soc.*, **117**, 3485 (1995).
[11] P. Singh, D.Y. Jeter, W.E. Hatfield, D.J. Hodgson. *Inorg. Chem.*, **11**, 1657 (1972).
[12] W.E. Marsh, W.E. Hatfield, D.J. Hodgson. *Inorg. Chem.*, **21**, 2679 (1982).
[13] O. Castillo, A. Luque, M. Julve, F. Lloret, P. Román. *Inorg. Chim. Acta*, **315**, 9 (2001).
[14] G.A. van Albada, S.A. Komaei, H. Kooijman, A.L. Spek, J. Reedijk. *Inorg. Chim. Acta*, **287**, 226 (1999).
[15] N. Lah, J. Koller, G. Giester, P. Segedin, I. Leban. *New J. Chem.*, **26**, 933 (2002).
[16] B.B. Koleva, E.N. Trendafilova, M.G. Arnaudov, W.S. Sheldrick, H. Mayer-Figge. *Transition Met. Chem.*, **31**, 866 (2006).
[17] J.A. Moreland, R.J. Doedens. *Inorg. Chem.*, **17**, 674 (1978).
[18] M.M. Turnbull, C.P. Landee, B.M. Wells. *Coord. Chem. Rev.*, **249**, 2567 (2005).
[19] L. Li, M.M. Turnbull, J. Ackers, J. Chen, H. Lin, B. Pan, H. Wang, B.M. Foxman. *Inorg. Chim. Acta*, **362**, 3845 (2009).
[20] A.J. Gale, C.P. Landee, M.M. Turnbull, J.L. Wikaira. *Polyhedron*, **52**, 986 (2013).
[21] L. Li, M.M. Turnbull, C.P. Landee, J. Jornet, M. Deumal, J.J. Novoa, J.L. Wikaira. *Inorg. Chem.*, **46**, 11254 (2007).
[22] *CrysAlisPro, Version 1.171.35.19*, Oxford Diffraction Ltd, Oxford (release 27-10-2011 CrysAlis171.NET).
[23] G.M. Sheldrick. *SADABS V 2.01: An Empirical Absorption Correction Program*, Bruker AXS, Madison, WI (1999).
[24] G.M. Sheldrick. *Acta Crystallogr., Sect. A: Found. Crystallogr.*, **64**, 112 (2008).
[25] R.L. Carlin. *Magnetochemistry*, Springer, Berlin (1986).
[26] D.A. McMorran, C.M. Hartshorn, P.J. Steel. *Polyhedron*, **23**, 1055 (2004).
[27] J.-Z. Gu, H.-Z. Kou, L. Jiang, T.-B. Lu, M.-Y. Tan. *Inorg. Chim. Acta*, **359**, 2015 (2006).
[28] M. Laing, G. Carr. *J. Chem. Soc. A: Inorg. Phys. Theor.*, 1141 (1971).
[29] K.C. Shortsleeves, L.N. Dawe, C.P. Landee, M.M. Turnbull. *Inorg. Chim. Acta*, **362**, 1859 (2009).
[30] M. Pinsky, D. Avnir. *Inorg. Chem.*, **37**, 5575 (1998).
[31] B.R. Landry, M.M. Turnbull, B. Twamley. *J. Chem. Crystallogr.*, **37**, 81 (2007).
[32] T. Fetzer, A. Lentz, T. Debaerdemaeker. *Z. Naturforsch., B: Chem. Sci.*, **44**, 553 (1989).
[33] F.F. Awwadi, R.D. Willett, S.F. Haddad, B. Twamley. *Cryst. Growth Des.*, **6**, 1833 (2006).
[34] G.W. Tremelling, B.M. Foxman, C.P. Landee, M.M. Turnbull, R.D. Willett. *Dalton Trans.*, 10518 (2009).
[35] T.J. Coffey, C.P. Landee, W.T. Robinson, M.M. Turnbull, M. Winn, F.M. Woodward. *Inorg. Chim. Acta*, **303**, 54 (2000).
[36] J. Anagnostis, M.M. Turnbull. *Acta Crystallogr., Sect. C: Cryst. Struct. Commun.*, **54**, 681 (1998).

[37] F.F. Awwadi, R.D. Willett, B. Twamley. *Cryst. Growth Des.*, **7**, 624 (2007).
[38] R.D. Willett, F. Awwadi, R. Butcher, S. Haddad, B. Twamley. *Cryst. Growth Des.*, **3**, 301 (2003).
[39] D. Johnston, R. Kremer, M. Troyer, X. Wang, A. Klümper, S. Bud'ko, A. Panchula, P. Canfield. *Phys. Rev. B*, **61**, 9558 (2000).
[40] B. Bleaney, K. Bowers. *Proc. R. Soc. A: Math. Phys. Eng. Sci.*, **214**, 451 (1952).
[41] S.N. Herringer, M.M. Turnbull, C.P. Landee, J.L. Wikaira. *Dalton Trans.*, 4242 (2011).
[42] V.H. Crawford, H.W. Richardson, J.R. Wasson, D.J. Hodgson, W.E. Hatfield. *Inorg. Chem.*, **15**, 2107 (1976).
[43] C.-J. Lin, J.-L. Qi, Y.-Q. Zheng, J.-L. Lin. *J. Coord. Chem.*, **66**, 3877 (2013).
[44] P. Wang, Y.-Y. Wang, Y.-H. Chi, W. Wei, S.-G. Zhang, E. Cottrill, J.-M. Shi. *J. Coord. Chem.*, **66**, 3092 (2013).
[45] F.F. Awwadi, R.D. Willett, K.A. Peterson, B. Twamley. *Chem.-Eur. J.*, **12**, 8952 (2006).
[46] F.F. Awwadi, R.D. Willett, K.A. Peterson, B. Twamley. *J. Phys. Chem. A*, **111**, 2319 (2007).